Bull. Mater. Sci., Vol. 36, No. 4, August 2013, pp. 505–511. © Indian Academy of Sciences.

Preparation and gas-sensing property of parallel-aligned ZnO nanofibrous films

ZIKUI BAI[a,*], WEILIN XU[a], CHANGSHENG XIE[b], MINGCHAO DONG[c], SHUNPING ZHANG[b], JIE XU[a] and SHILI XIAO[a]

[a]Key Lab for Green Processing and Functionalization of New Textile Materials, Ministry of Education, Wuhan Textile University, Wuhan 430073, P.R. China

[b]State Key Laboratory of Material Processing and Die and Mould Technology, Huazhong University of Science and Technology, Wuhan 430074, P.R. China

[c]Zhuxi County Environmental Protection Agency, Shiyan 442300, P.R. China

MS received 13 October 2011; revised 24 April 2012

Abstract. **Parallel-aligned zinc oxide (ZnO) nanofibrous films fabricated by using electrospinning technique were used in gas sensors for the detection of ethanol and formaldehyde. The morphologies and crystal structures of the films were characterized by field-emission scanning electron microscopy (FE–SEM) and X-ray diffraction (XRD), respectively. FE–SEM results showed that ZnO nanofibres had an approximate diameter of 100–300 nm and consisted of hexagonal wurtzite structure ZnO nanocrystals with a primary particle diameter of 20–50 nm. The results of resistance–temperature characteristics and responses to ethanol and formaldehyde indicated that the parallel-aligned ZnO nanofibrous film had a low activation energy (0·246 eV), a low optimum operating temperature and a high response. The response and recovery had a high rate in the initial stage and a low rate in the later stage. The parallel-aligned ZnO nanofibrous film had excellent potential application for formaldehyde sensor.**

Keywords. **ZnO; parallel-aligned nanofibrous film; electrospinning; sensing characteristics.**

1. Introduction

Zinc oxide (ZnO), which is an interesting chemically and thermally stable *n*-type semiconductor with a large exciton binding energy (60 meV) and a large bandgap (3·37 eV) energy, has many significant technological applications such as photocatalysts (Chakrabarti and Dutta 2004), solar cells (Baxter and Aydil 2006; Pradhan *et al* 2007), transparent conductive films (Park *et al* 2006; Ma *et al* 2007), gas sensors (Zhu *et al* 2004; Ge *et al* 2007a) and so on. A wide variety of nanostructure ZnO, such as nanowires (Yang *et al* 2004), nanowalls (Heo *et al* 2004; Wu *et al* 2005; Zhang *et al* 2006), nanobelts (Wang 2003), nanorods (Gao and Wang 2005), nanosheets (Chen *et al* 2005), nanofibres (Yang *et al* 2007; Wu *et al* 2009) and so on, have been fabricated. Recently, one-dimensional ZnO nanostructures have attracted much attention in gas-sensing since the dimension and surface-to-volume ratio can greatly influence the material performance (Wu *et al* 2009; Hongsith *et al* 2010). Considerable efforts have been made to fabricate ZnO nanowires, nanobelts, nanorods and nanofibres via thermal oxidation, thermal evaporation, self-catalytic growth, molten salt synthesis and electrospinning (Wang 2003; Yang *et al* 2004; Gao and Wang 2005; Yang *et al* 2007; Wu *et al* 2009). Among these methods, electrospinning has been proved to be a versatile and effective method for manufacturing a nanoscale fibre.

Common to the reports is that for the fabrication of electrospun ZnO nanofibre gas sensors, ZnO nanofibres must be removed from a substrate and be transferred into a paste by mixing with distilled water or organic vehicle and grinding, and then dispersed randomly onto a sensor substrate (Wang *et al* 2010), as our previous fabrication of ZnO thick film gas sensor (Zhu *et al* 2005). This "pick-and-place" process will damage the morphology of nanofibres to form ZnO rods and/or particles. It is not accurate that the sensor responses were discussed according to the morphology of raw fibres. However, by using the electrospinning process for the fabrication of nanofibre sensors, it was only reported that "pick" step was eliminated as it allowed a direct placement of nanofibres onto a sensor chip (Wu *et al* 2009). The obtained film had a non-woven structure consisting of ZnO nanofibres and was isotropic in-plane. The nanofibre had a large length-to-diameter ratio to facilitate fast mass transfer of gas molecules to the interaction region as well as to improve the rate for charge carriers to transverse the barriers induced by molecular recognition along the fibres (Kolmakov and Moskovits 2004). So the alignment of ZnO nanofibres had an important effect on the gas-sensing response of sensor. The parallel alignment of ZnO nanofibres is to improve the gas-sensing response of sensor.

*Author for correspondence (zkbwn@163.com)

Substantial efforts have been devoted in recent years to the development of methods to achieve parallel-aligned nanofibres (Chew *et al* 2006). Conventional collection method of nanofibres on the surface of a rotating drum or mandrel can produce thick nanofibrous sheets (Matthews *et al* 2002), but typically results in only partial nanofibre alignment, even at very high rotation velocities. Nanofibre deposition onto the edge of a rotating disc (essentially a narrow mandrel) resulted in a band of nanofibres with relatively high alignment (Kim *et al* 2003). Wu *et al* invented a modified electrospinning method to fabricate the highly oriented zinc oxide nanofibre bundle (Wu *et al* 2007). However, it is difficult for the alignment of nanofibrous sheets or films fabricated by using this method to meet the electronic components. Several alignment methods based on electrical forces acting on charged jet segments have been explored recently (Dersch *et al* 2003; Li *et al* 2003; Dzenis 2004). One of the best methods is to use rectangular frame electrodes (Dersch *et al* 2003; Dzenis 2004) to produce parallel-aligned nanofibrous films. However, the parallel-aligned ZnO nanofibre sensor fabricated by using electrospinning technology was rarely reported.

In this study, we designed a parallel grid collector consisting of parallel aluminum wire to fabricate the parallel-aligned zinc acetate/PVA composite nanofibrous films, which were entwined closely onto a ceramic tube and then were calcined to obtain the parallel-aligned ZnO nanofibrous film sensors. Surface morphology, microstructure and gas sensing characteristics were systematically investigated.

2. Experimental

2.1 *Materials*

All chemicals used in the experiment were of analytical grade. Polyvinyl alcohol (PVA, Mn = 80000, analytical grade) was supplied by Chuanwei Co. Ltd. Zinc acetate ($Zn(CH_3COO)_2{\cdot}2H_2O$) and acetic acid ($CH_3COOH$) were obtained from Sinopharm Chemical Reagent Co. Ltd. Distilled water was used as a solvent.

2.2 *Preparation of precursor solution*

In this procedure, 5 g of PVA beads and 1·563 g of zinc acetate were mixed with 45 ml distilled water (The mass ratio of zinc acetate/PVA was an optimum value). Then, under vigorous stirring, this solution was heated to 98 °C with a heating rate of 1 °C/min and held for 4 h. Subsequently, 0·5 ml of acetic acid solution (0·1 mol/L) was added into the above solution under vigorous stirring for 10 min, inhibiting the formation of zinc hydroxide. Thus, transparent viscous gel of zinc acetate/PVA was obtained.

2.3 *Preparation of parallel-aligned nanofibrous films*

Schematic diagram of the electrospinning apparatus is shown in figure 1, which consisted of three major components: a spinneret, a collector and a high voltage power. The spinneret was a 5 ml syringe (the inner diameter of the stainless needle, 0·45 mm) that connected to a syringe pump. The positive lead from a high voltage supply was connected to the external surface of needle via an alligator clip. The collector was a parallel grid consisting of parallel aluminum wire. Previous optimization work had been done in deciding the electrospinning deposition conditions (distance needle-collector, voltage and flow rate). Distance between the needle and the collector was 10 cm. The transparent viscous gel of zinc acetate/PVA was loaded into a 5 ml plastic syringe. The flow rates were controlled by the syringe pump (0·08 ml/h). Voltage of 20 kV was applied to the needle. The transparent viscous gel of zinc acetate/PVA was electrospun onto the parallel grid collector to obtain a parallel-aligned zinc acetate/PVA composite nanofibrous film between the parallel aluminum wires.

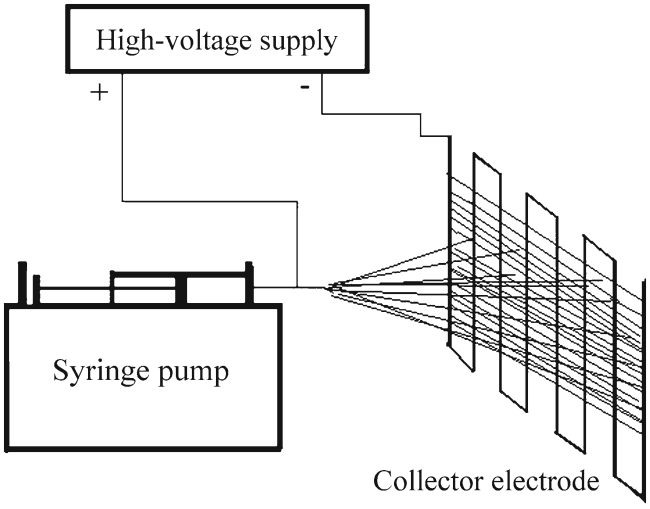

Figure 1. Schematic diagram of electrospinning apparatus.

2.4 *Sensor preparation and measurement*

The as-prepared zinc acetate/PVA composite nanofibrous films were enwound closely onto a ceramic tube with a pair of annular gold electrodes. To obtain close adhesion between the zinc acetate/PVA composite nanofibrous films and the annular gold electrodes, Ag paste was painted on the nanofibrous films present at the end of the ceramic tube. The obtained samples were conserved in air for 24 h and then dried at 80 °C for 6 h. The ceramic tube with nanofibrous films was subsequently heated with a rate of 2 °C/min from room temperature to 650 °C in a tubular silica furnace in air and calcined for 4 h at 650 °C to obtain the parallel-aligned nanofibrous film gas sensor. A small Ni–Cr alloy wire was placed through the tube as a heater, which provided operating temperature. In order to improve their stability, the gas sensors were aged at 400 °C for 3 days in air. Schematic illustration of the sensor structure is shown in figure 2(a).

Gas-sensing properties of the sensor were measured on a static system in laboratory condition (25 °C, 80%

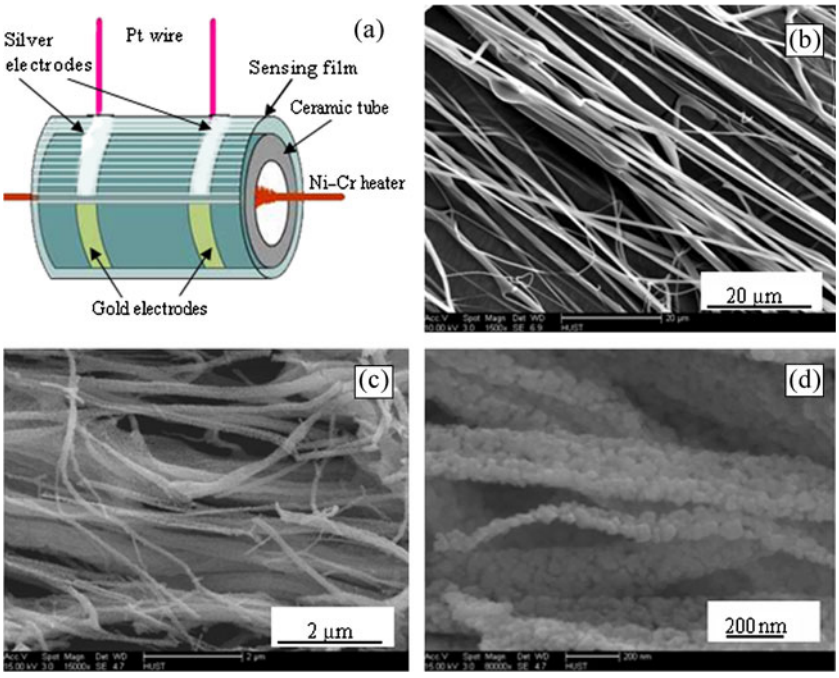

Figure 2. (**a**) Schematic illustration of sensor structure, SEM images of fibres before being sintered (**b**), after being sintered (**c**) and high magnification (**d**).

relative humidity). The experimental procedure was described in detail in the literature (Zhu *et al* 2005). The detected vapours were ethanol and formaldehyde (concentration, 100 ppm). The gas response (S) is given by $S = R_a/R_g$, where R_a and R_g are the resistance of the sensor in air and in detected gas, respectively.

2.5 *Characterization*

In X-ray diffraction analysis (XRD), the sample was fixed onto a stub and placed within the chamber of analytical X-ray powder diffractometer (X'Pert Pro, PANalytical Holland, wavelength 1·54 Å, CuKα_1 radiation). The morphologies of the films were observed by a Sirion II type field-emission scanning electron microscope (FE–SEM, FEI, Holland).

3. Results and discussion

3.1 *Morphologies and structures of parallel-aligned nanofibrous films*

Figure 2(b) shows typical FE–SEM images of the parallel-aligned zinc acetate/PVA composite nanofibrous films, while figures 2(c) and (d) show morphologies of ZnO parallel-aligned nanofibrous films. The parallel grid collector consisting of the parallel aluminum wire had the same effect as the rectangular frame electrodes to obtain the parallel-aligned nanofibrous films (Dersch *et al* 2003). Zinc acetate/PVA composite fibres with a smooth surface morphology had a diameter of 1–2 μm. After calcination, diameter of ZnO nanofibre shrank drastically to 100–300 nm, as shown in figures 2(c) and (d). The shrinkage of fibres was due to the burn-out of PVA from the nanofibres and the crystallization of ZnO phase during calcination process. Although PVA was fully decomposed, the parallel-aligned fibre structure was still retained. It contributed to the low heating rate (2 °C/min). Figure 1(d) shows that the ZnO nanofibres consisted of granular crystallites with a primary particle diameter of 20–50 nm and mesopores with a diameter of 5–10 nm. PVA pre-occupied spaces could contribute to the

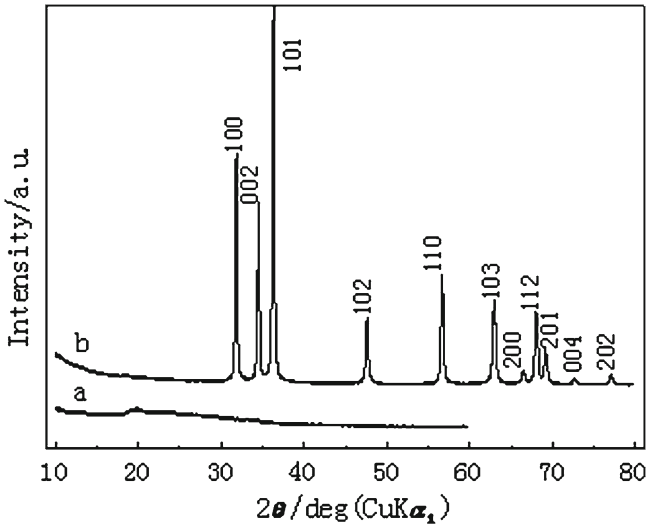

Figure 3. XRD patterns of zinc acetate/PVA composite fibres before (**a**) and after (**b**) calcination.

formation of the pores. Moreover, the pore structures could also be related to the crystalline phase growth as the calcination temperature was raised (Chen *et al* 2008).

Figure 3 shows XRD patterns of zinc acetate/PVA composite fibres before and after calcination. Figure 3(a) shows only a broad peak at $2\theta = 20°$, indicating that the zinc acetate/PVA composite fibres were amorphous. After annealing at 650 °C, the strong and sharp diffraction peaks obtained could be well indexed to hexagonal wurtzite structure ZnO (JCPDS: 89-0510, figure 3(b)). No other diffraction peaks were observed, which indicated that the sintered sample was high-purity ZnO. Referring the main peak (101) of wurtzite phase, the grain size of ZnO estimated from Scherrer's formula was about 40 nm, which was entirely consistent with the result in figure 2(d). This indicated that the nanofibres consisted of nanocrystalline ZnO.

3.2 *Electrical conductivities of parallel-aligned ZnO nanofibrous films*

Figure 4 shows Arrhenius plots of the parallel-aligned ZnO nanofibrous film in air. If the electrical conduction of ZnO nanofibres was thermally assisted, the conductivity (σ) could be depicted as $\sigma = \sigma_0 \exp(-E_a/k_b T)$, where E_a, k_b and T were the activation energy, Boltzmann constant ($= 8{\cdot}62 \times 10^{-5}$ eV/K) and absolute temperature, respectively (Mott and Davis 1979). In such a case, the data could be fitted to a straight line and the average activation energy of surface chemisorbed oxygen could be deduced from the slope of the straight line. The apparent activation energy derived from this plot was 0·246 eV, which was much lower than that of the non-woven structure nanofibrous film (0·33 eV) (Park *et al* 2009) and was much higher than that of the single nanorod (0·089 eV) (Heo *et al* 2004). The smaller the activation energy was, the more active surface absorption was. The change of resistance, largely depending on the operating temperature, indicated that the resistance of the films were controlled by surface effects.

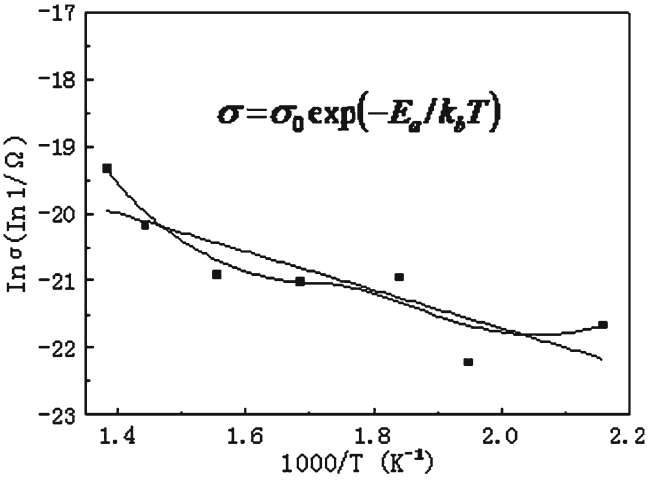

Figure 4. Arrhenius plots of parallel-aligned ZnO nanofibrous film.

The electrical conductivity of polycrystalline metal oxides was mainly governed by the potential barrier formed at grain boundaries (GBs) and the electrical conduction occurred along percolation paths via GB contacts (Gupta 1990). The activation value represented Schottky barriers formed at GBs. In this study, ZnO nanofibres consisting of granular crystallites with a diameter of 20–50 nm composed of the sensing film (figure 2(d)). The grain boundaries along the fibre were different from the fibre-to-fibre grain boundaries. The parallel-aligned ZnO nanofibrous film was highly anisotropic in-plane. The parallel-aligned ZnO nanofibres bridged between the two electrodes of the device. The direction of the test current was parallel to the fibre axis. As a result, charges in a parallel-aligned nanofibrous film would be limited to traversing only across grain boundaries along the fibres, with the shortest transmission path. So, the parallel-aligned nanofibrous film has a low activation energy (0·246 eV). It is confirmed that the grain boundary along the fibre had a smaller barrier than the fibre-to-fibre grain boundaries (Ra *et al* 2005; Leslie *et al* 2009; Zhou *et al* 2009). Charges in a non-woven structured nanofibrous film would be forced to traversing across the fibre-to-fibre grain boundaries between the two electrodes of the device. The total transport barriers in charge-transport pathways were increased. So, the non-woven structure of nanofibrous film (0·33 eV) had a higher activation value than the parallel nanofibrous film (0·246 eV). The single nanorod had a low activation value (0·089 eV $\pm$ 0·02 eV) and it is possible that the conduction is surface-related, as in UV photo-response measurements (Heo *et al* 2004).

3.3 *Gas sensing properties of parallel-aligned ZnO nanofibrous films*

The responses of the parallel-aligned ZnO nanofibrous film to ethanol and formaldehyde (concentration, 100 ppm) as a function of operating temperature are shown in figure 5. It was obvious that the responses increased with the increase in operating temperature in low temperature range, reached the maxima at 240 °C and 270 °C to ethanol and formaldehyde, respectively and began to decrease above this temperature.

The change in response was mainly induced by the adsorption and desorption of gas molecules from a surface of film at testing temperature (Huang *et al* 2004). In air environment, oxygen molecules were generally chemisorbed onto the surface of the ZnO in forms of O_2^-, O^- and O^{2-}. The decrease in carrier concentration within ZnO caused resistance of the film to increase. When the film was exposed to reducing gas (i.e. ethanol and formaldehyde), the surface oxygen species (oxygen ions O_2^-, O^- and O^{2-}) reacted with reducing gas and electrons were released into the conduction band of ZnO, thus increasing the carrier concentration and ultimately resulting in the decrease in resistance of the film. Obviously, the film with higher specific surface area could adsorb more

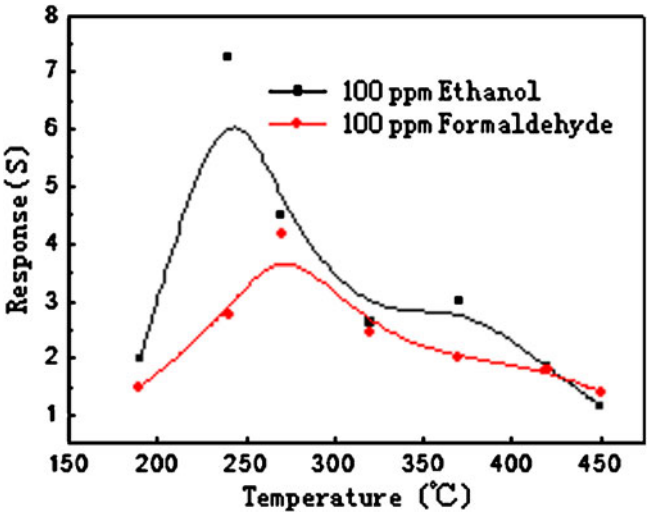

Figure 5. Response of parallel-aligned ZnO nanofibrous film-based sensor with operating temperature.

oxygen molecules, thus possessing higher concentration of oxygen ions. It was noteworthy that the oxygen-adsorption reaction was exothermic (Chang *et al* 2002). At the temperature above an optimum temperature, the basic reaction $\left(\frac{1}{2}O_2\,(g) + e^- \rightarrow O^-_{ads}\right)$ would proceed to the left, which led to the decrease of trapped electrons from the conduction band and the decrease of the oxygen ion concentration in the film. Therefore, the response decreased.

The optimum temperature of the film was related to the surface morphology and microstructure characteristics of the film. In this study, the parallel-aligned ZnO nanofibrous film to ethanol had a lower optimum temperature (240 °C) than the non-woven structured ZnO nanofibrous film (300 °C) (Wang *et al* 2010). For formaldehyde, the optimum temperature of the parallel-aligned ZnO nanofibrous film was 270 °C, which was lower than that of ZnO nanopowder film (460 °C) (Ge *et al* 2007b; Bai *et al* 2008). It was generally proposed that the parallel-aligned ZnO nanofibrous film exhibited a higher surface-to-volume ratio (Wang *et al* 2006), thus provided more sites for adsorption of analyte molecules and made the absorption of analyte molecules on the surface of the film easily. In addition, the parallel-aligned ZnO nanofibrous film had low activation energy (0·246 eV). The change in responses with operating temperature was related to the activation energy of surface chemisorbed oxygen, which reflected the ability of interaction between surface chemisorbed oxygen and adsorbed gas. The activation energy was inversely proportional to the oxygen adsorption capacity (Jiao *et al* 2002). The difference in the responses of the films to ethanol and formaldehyde might be related to the different chemical bonds (Ge *et al* 2007a, b). The parallel-aligned ZnO nanofibrous film had a lower optimum temperature and higher response than ZnO nanopowder film. This result showed that the parallel-aligned ZnO nanofibrous film had excellent potential application for formaldehyde sensor.

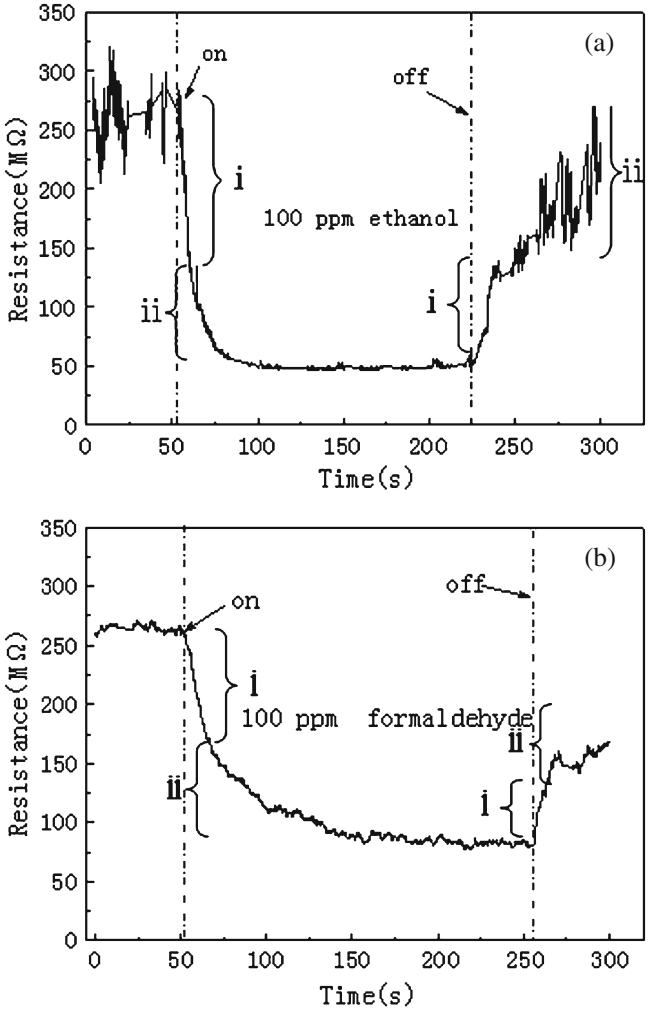

Figure 6. Response–recovery curves of parallel-aligned ZnO nanofibre based sensor to ethanol (**a**) and formaldehyde (**b**), (i) in initial stage and (ii) later stage.

It is well known that the response and recovery behaviour is one of the most important characteristics for evaluating the performance of gas sensors. The sensor response time was defined as the time required until 90% of the response resistance was reached after the film was in contact with the detected gas. The recovery time denoted the time needed until 90% of the original resistance was recovered after the detected gas was removed. The resistances of the parallel-aligned ZnO nanofibrous film to 100 ppm ethanol at 240 °C and to 100 ppm formaldehyde at 270 °C as a function of time are shown in figures 6(a) and (b), respectively which had similar response–recovery characteristics. The response and recovery times of the parallel-aligned ZnO nanofibrous film were longer than that of the non-woven structured ZnO nanofibrous film (Wang *et al* 2010) and the tetrapod-shaped ZnO nanoparticles film (Zhu *et al* 2005). It was noteworthy that the response and recovery process could be divided into two different rate processes, which were a high rate in the initial stage (i) and a low rate in the later stage (ii) as shown in figure 6.

The response and recovery of the sensor corresponded to the reducing gas diffusion and oxidation in the film. The diffusion time of the reducing gas, which was related to microstructure of the film, dominated the response time. The diffusion contribution to total molecular transport through the pore material depended on pore size and length of the path along which the molecule travelled (Ahmad *et al* 2003; Korotcenkov 2008). The sensor had a fast response and recovery in the initial stage because the diffusion of the reducing gas (i.e. ethanol and formaldehyde) occurred in the big pores between ZnO nanofibres. The nanofibres prepared by using electro-spinning technology had a high surface-to-volume ratio (Wang *et al* 2005, 2006) and a large length-to-diameter ratio. The reducing gas (i.e. ethanol and formaldehyde) could be adsorbed on the surface of the nanofibres quickly. At the same time, the large length-to-diameter ratio of the nanofibres could facilitate fast mass transfer of the reducing gas molecules to the interaction region as well as to improve the rate for charge carriers to cross the barriers induced by molecular recognition along the fibres (Kolmakov and Moskovits 2004; Li *et al* 2008). In the later stage, slow response and recovery behaviour of the sensor could be attributed to the reaction taking place inside ZnO fibres with 5–10 nm diameter mesopores. The sluggish gas diffusion through the pores between the primary nanoparticles greatly decreased the response speeds. When reducing gas (i.e. ethanol and formaldehyde) was removed, recovery of the resistance was determined by both oxygen re-adsorption from the ambient to the surface and re-oxidation of the oxide (Chang *et al* 2002). For small molecule O_2, effect of the film microstructure on the oxygen re-adsorption rate was quite small. The re-oxidation of the oxide was to form chemisorbed oxygen (oxygen ions O_2^-, O^- and O^{2-}) in the oxide surface. The re-oxidation processes were the sluggish surface reactions regarding adsorption, dissociation and ionization of oxygen (Choi *et al* 2010). The different response and recovery of the parallel-aligned ZnO nanofibrous film to ethanol and formaldehyde might be due to the diffusion characteristic difference and different chemical bonds of ethanol and formaldehyde (Ge *et al* 2007a).

4. Conclusions

Parallel-aligned ZnO nanofibrous films fabricated by using electrospinning technique were used in gas sensors for the detection of ethanol and formaldehyde. The ZnO nanofibres had an approximate diameter of 100–300 nm and consisted of hexagonal wurtzite structure ZnO nanocrystals with a primary particle diameter of 20–50 nm. The results of the resistance–temperature characteristics and the responses to 100 ppm ethanol and formaldehyde indicated that the parallel-aligned ZnO nanofibrous film had low activation energy (0·246 eV), a low optimum operating temperature and a high response. The parallel-aligned ZnO nanofibrous film had excellent potential application for formaldehyde sensor. The response and recovery had a high rate in the initial stage and a low rate in the later stage. This work helps us to understand that the microstructure optimization of the gas sensor should focus not only on the surface morphologies and the size of particles that composed of a film but also on the arrangement between particles.

Acknowledgements

This work was supported by 973 project of China (No. 2012CB722701), the Natural Science Foundation of Hubei province (No. 2012FFB04603) and the Natural Science Foundation of Wuhan Textile University. The authors are also grateful to Analytical and Testing Centre of Huazhong University of Science and Technology.

References

Ahmad A, Walsh J and Wheat T A 2003 *Sens. Actuators* **B93** 538
Bai Z K, Xie C S, Hu M L and Zhang S P 2008 *Physica* **E41** 235
Baxter J B and Aydil E S 2006 *Sol. Energy Mater. Sol. Cells* **90** 607
Chakrabarti S and Dutta B K 2004 *J. Hazard. Mater.* **112** 269
Chang J F, Kuo H H, Leu I C and Hon M H 2002 *Sens. Actuators* **B84** 258
Chen S J, Liu Y C, Shao C L, Mu R, Lu Y M, Zhang J Y, Shen D Z and Fan X W 2005 *Adv. Mater.* **17** 586
Chen J Y, Chen H C, Lin J N and Kuo C S 2008 *Mater. Chem. Phys.* **107** 480
Chew S Y, Wen Y, Dzenis Y and Leong K W 2006 *Curr. Pharm. Des.* **12** 4751
Choi J K, Hwang I S, Kima S J, Parkb J S, Park S S, Jeong U, Yun C K and Lee J H 2010 *Sens. Actuators* **B150** 191
Dersch R, Liu T, Schaper A K, Greiner A and Wendorff J H 2003 *J. Polym. Sci. Part A: Polym. Chem.* **41** 545
Dzenis Y 2004 *Science* **304** 1917
Gao T and Wang T H 2005 *Appl. Phys.* **A80** 1451
Ge C Q, Xie C S and Cai S Z 2007a *Mater. Sci. Eng.* **B137** 53
Ge C Q, Xie C S, Zeng D W and Cai S Z 2007b *J. Am. Ceram. Soc.* **90** 3263
Gupta T 1990 *J. Am. Ceram. Soc.* **73** 1817
Heo Y W, Norton D P, Tien L C, Kwon Y, Kang B S, Ren F, Pearton S J and LaRoche J R 2004 *Mater. Sci. Eng. Rep.* **47** 1
Hongsith N, Wongrat E, Kerdcharoen T and Choopun S 2010 *Sens. Actuators* **B144** 67
Huang X J, Meng F L, Pi Z X, Xu W H and Liu J H 2004 *Sens. Actuators* **B99** 444
Jiao Z, Chen F and Li M Q 2002 *J. Inorg. Mater.* **17** 316
Kim K, Yu M, Zong X H, Chiu J, Fang D F and Seo Y S 2003 *Biomaterials* **24** 4977
Kolmakov A and Moskovits M 2004 *Annu. Rev. Mater. Res.* **34** 151
Korotcenkov G 2008 *Mater. Sci. Eng. R* **61** 1
Leslie H J, Michael F T, Iain M, Martin H and Alberto S 2009 *Adv. Mater.* **21** 1568
Li D, Wang Y and Xia Y 2003 *Nano Lett.* **3** 1167
Li Z Y, Zhang H N, Zheng W, Wang W, Huang H M, Wang C, MacDiarmid A G and Wei Y 2008 *J. Am. Chem. Soc.* **130** 5036
Ma Q B, Ye Z Z, He H P, Zhu L P, Wang J R and Zhao B H 2007 *Mater. Lett.* **61** 2460

Matthews J A, Wnek G E, Simpson D G and Bowlin G L 2002 *Biomacromolecules* **3** 232

Mott N and Davis E 1979 *Electronic process in non-crystalline materials* (Oxford: Clarendon) 2nd ed.

Park S, Ikegami T, Ebihara K and Shin P K 2006 *Appl. Surf. Sci.* **253** 1522

Park J A, Moon J, Lee S J, Lim S C and Zyung T 2009 *Curr. Appl. Phys.* **9** S210

Pradhan B, Batabyal S K and Pal A J 2007 *Sol. Energy Mater. Sol. Cells* **91** 769

Ra E J, An K H, Kim K K, Jeong S Y and Lee Y H 2005 *Chem. Phys. Lett.* **413** 188

Wang Z L 2003 *Adv. Mater.* **15** 432

Wang H T, Kang B S, Ren F, Tien L C, Sadik P W, Norton D P, Pearton S J and Lin J S 2005 *Appl. Phys. Lett.* **86** 243503

Wang C H, Chu X F and Wu M M 2006 *Sens. Actuators* **B113** 320

Wang W, Li Z Y, Zheng W, Huang H M, Wang C and Sun J H 2010 *Sens. Actuators* **B143** 754

Wu G S, Xie T, Yuan X Y, Li Y, Yang L, Xiao Y H and Zhang L D 2005 *Solid State Commun.* **134** 485

Wu H, Lin D, Zhang R and Pan W 2007 *J. Am. Ceram. Soc.* **90** 632

Wu W Y, Ting J M and Huang P J 2009 *Nanoscale Res. Lett.* **4** 513

Yang X, Shao C, Guan H, Li X and Gong J 2004 *Inorg. Chem. Commun.* **7** 176

Yang M, Xie T, Peng L and Zhao Y 2007 *Appl. Phys.* **A89** 427

Zhang Y, Yu K, Ouyang S and Zhu Z 2006 *Mater. Lett.* **60** 522

Zhou Z P, Lai C L, Zhang L F, Qian Y, Hou H Q and Fong D H 2009 *Polymer* **50** 2999

Zhu B L, Xie C S, Wang W Y, Huang K J and Hu J H 2004 *Mater. Lett.* **58** 624

Zhu B L, Xie C S, Wang A H, Zeng D W, Song W L and Zhao X Z 2005 *Mater. Lett.* **59** 1004